Case Studies in Thermal Engineering 39 (2022) 102441

Contents lists available at ScienceDirect

Case Studies in Thermal Engineering

journal homepage: www.elsevier.com/locate/csite

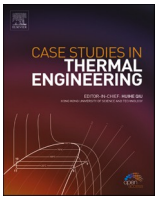

Heat transfer and pressure drop characteristics of ZnO/DIW based nanofluids in small diameter compact channels: An experimental study

Habib-ur-Rehman Siddiqi [a], Adnan Qamar [a,*], Rabia Shaukat [a], Zahid Anwar [a], Muhammad Amjad [a], Muhammad Farooq [a], Muhammad Mujtaba Abbas [a,**], Shahid Imran [a], Hassan Ali [b], T.M.Yunus Khan [c], Fahad Noor [a], Hafiz Muhammad Ali [d], M.A. Kalam [e], Manzoore Elahi M. Soudagar [f,g]

[a] Department of Mechanical, Mechatronics and Manufacturing Engineering, New-Campus, University of Engineering and Technology Lahore, Lahore, Pakistan
[b] De Montfort University Leicester, United Kingdom, Dubai Campus, Dubai International Academic City, Post Box: 294345, Dubai, United Arab Emirates
[c] Department of Mechanical Engineering, College of Engineering, King Khalid University, Abha, 61421, Saudi Arabia
[d] Mechanical Engineering Department, College of Engineering and Physics, King Fahd University of Petroleum and Minerals, Dhahran, Saudi Arabia
[e] Faculty of Engineering and IT, University of Technology, Sydney, Australia
[f] Department of Mechanical Engineering and University Centre for Research & Development, Chandigarh University, Mohali, 140413, Punjab, India
[g] Department of Mechanical Engineering, School of Technology, Glocal University, Delhi-Yamunotri Marg, Uttar Pradesh 247121, India

ARTICLE INFO

Keywords:
Aqueous
Heat transfer
Minichannel
Nanoparticles
Nanofluids
Pressure drop
Zinc oxide

ABSTRACT

This experimental study is focused on heat transfer performance and pressure drop characteristics of ZnO/DIW-based nanofluids (NFs) in horizontal mini tubes of different (1.0–2.0 mm) diameters. Different mass concentrations (0.012–0.048 wt %) of nanoparticles (NPs) were tested with varying fluid flow rates (12–24 ml/min) of NFs. The thermal conductivity (TC) and viscosity (VC) of stable NFs were tested at 20–60 °C, at a fixed temperature (40 °C), and concentration of NPs (0.048 wt%) the maximum rise was 18.27% and 20.31%, respectively. The local and average heat transfer coefficients (HTCs) and the pressure gradient were noticed to be directly proportional to volume flow rate of NFs and the mass concentration of NPs. However, an inverse trend was noticed with the test section's diameter. At 0.048 wt % of NPs and 24.0 ml/min flow rate of NFs, the maximum rise in local and average HTCs and pressure gradient was 17.11–11.61% and 13.05–9.79%, and 29.19–12.25%, respectively, in a tube's diameter of 1.0–2.0 mm. The friction factor increased with NP's loading while the same reduced with the fluid flow rate. The corresponding maximum change in the friction factor was 28.85–12.72% for the tubes with 1.0–2.0 mm diameters, respectively, at a 12.0 ml/min flow rate of NFs. The comparison of experimental findings for the HTCs, pressure gradients and friction factors with the standard Shah and Darcy's correlations showed that the observations are in good agreement with the predicted ones.

* Corresponding author. Department of Mechanical, Mechatronics and Manufacturing Engineering, New-Campus, University of Engineering and Technology Lahore, Lahore, Pakistan.
** Corresponding author. Department of Mechanical, Mechatronics and Manufacturing Engineering, New-Campus, University of Engineering and Technology Lahore, Lahore, Pakistan.
E-mail addresses: adnan@uet.edu.pk (A. Qamar), m.mujtaba@uet.edu.pk (M.M. Abbas).

https://doi.org/10.1016/j.csite.2022.102441
Received 23 June 2022; Received in revised form 14 September 2022; Accepted 18 September 2022
Available online 28 September 2022

Nomenclature:

A	cross sectional area of test section (m^2)
C_p	specific heat capacity (J/kg K)
Di	inner diameter (m)
Do	outer diameter (m)
f	friction factor (−)
h	heat transfer coefficient (W/m^2 K)
k	thermal conductivity (W/m K)
L	length of the test section (m)
Nu	Nusselt number (−)
Pr	Prandtl number (−)
ΔP	Pressure drop (Pa)
Q	heat applied (W)
Q''	heat flux (W/m^2)
Re	Reynolds number (−)
T	temperature (K)
T_{bf}	bulk fluid temperature (K)
u	velocity (m/s)
x	axial distance (m)

Greek symbols

Ø	volume fraction (−)
ρ	density (kg/m^3)
μ	viscosity (mPa s)
β	diffraction peak (Θ)

Subscripts

bf	base fluid
in	inlet
iw	inner wall
nf	nanofluid
np	nanoparticle
os	outer surface

1. Introduction

Rapid advancement have been made in electronic communications devices, compact heat exchangers, evaporators, and condensers in the last few decades. The exponential technological growth does brought a severe problem in thermal management for effective device operations. Researchers have used various conventional and non-conventional techniques [1,2] to cope demand. The literature has indicated that traditional practices are insufficient for removing surplus heat from modern high heat dissipating systems. The suspension of NPs in conventional base fluids (BFs), commonly known as NFs, could be a good solution for withstanding high heat dissipation from modern compact devices. NFs usually have higher thermal conduction and could have better thermal performance [3,4]. Therefore, NFs could be a potential candidate for managing high heat fluxes in electronic systems, chillers, refrigeration systems, automotive cooling, solar thermal systems and cooling and heating of buildings [5].

Micro and minichannel heat exchangers have received much attention recently because of their efficient thermal performance, large surface area, and small physical dimensions [6]. Numerous studies have investigated the thermal performance of micro and minichannels employing traditional heat transfer fluids (HTFs). However, the existing literature lacks studies addressing the in-depth investigations on the heat transfer performance of micro and minichannels with aqueous metal oxide-based NFs [7,8].

The NFs integration with the microchannel heat exchangers has improved the system's thermal performance [9]. Hwang et al. [10] worked with aqueous-based Al_2O_3 NFs having different mass concentrations (0.01–0.30 wt %) of NPs in a small test section with a 1.812 mm inside diameter. At a constant Reynolds number, they observed up to 8.0% enhancement in HTCs with 0.30 wt% of NPs compared to pure BFs. Karimzadehkhouei et al. [11] studied aqueous-based NFs with Al_2O_3 and TiO_2 NPs having a 20 nm mean diameter in a small horizontal tube with 717 μm inside diameter with varying Reynolds numbers under thermally and hydrodynamically developing flow conditions. At Reynolds numbers more than 1200, the increase in NPs loading significantly affected HTC. Upto 25% enhancement in HTCs was reported for tests when Reynolds numbers >1500. Wen et al. [12] analyzed heat transfer and friction factors of aqueous ZnO NFs with 0.75–1.5 wt% of NPs through a small tube of 1.59 mm inside diameter. For 1.50 wt% of NPs, 10.50% enhancement in HTC was reported. However, the friction factor intensified up to 40.90% due to the possible rise in the

viscosity of the NFs. Lodhi et al. [13] analyzed the thermal behaviour of NFs in a microchannel heat sink having 500 μm inside diameter using aqueous-based Al_2O_3 NFs within 1.0–3.0 wt % concentration of NPs, and Reynolds numbers ranging from 300 to 1000. At NPs concentration of 3.0 wt % an enhancement of 24.5% and 22.7% in HTC, and friction factor under similar operating conditions were observed. Thermophysical properties of aqueous-based Al_2O_3 and TiO_2 NFs were studied in a small horizontal test section by Azari et al. [14]. Their observation showed that the HTCs significantly increased at low/dilute concentration of Al_2O_3 and TiO_2 NPs. An enhancement of 16% and 28% in HTC were found with Al_2O_3 NFs.

Almohammadi et al. [15] used aqueous-based Al_2O_3 NFs in a small circular test section to examine their thermal performance. Experimental data showed a 27.0% increment in HTCs for 1.0 vol % of NPs. Nguyen et al. [16] experimented with Al_2O_3/DIW base NFs at a 6.80% volume fraction of NPs in a heat exchanger and obtained a 40.0% enhancement in the HTC. Behi et al. [17] tested Al_2O_3/DW-based NFs in a small diameter test section under different Reynolds numbers and found an enhancement of 42.0% for 5.5 vol % of NPs. Esfahany and Fotukian [18] observed a 25.0% and 20.0% augmentation in HTC and pressure gradient across the compact channel heat exchanger. The heat-carrying capacity of water base Al_2O_3 NFs in compact channels of various geometrical sizes was investigated by Saeed and Kim [19]. It was found in their study that the HTC strongly depends upon the concentration of NPs within the host BFs. Aqueous-based ZnO NFs were tested for thermal performance in a car radiator [20]. The results demonstrated that by raising the fraction of NPs within the BFs, 46.0% HTC intensification has been found. Arshad and Ali [21] investigated the TiO_2 NFs, in a microchannel with a 1.0 mm inner diameter under heating power input of 100W, 125W and 150W, respectively. The maximum HTC of TiO_2 NFs was 12.75% at lower heating power. The cooling ability of the aqueous-based Al_2O_3 NFs in a copper tube was investigated by Sohel et al. [22] at two different volume flow rates. Results concluded that the thermal efficiency of Al_2O_3/DIW NFs intensified within the range of 0.1–0.25% volume concentrations of NPs under laminar flow conditions. An improvement of 18.0% in HTC was observed at a 0.25 vol % fraction of NPs.

Isfahani and Afrand [23] conducted an experimental and numerical investigation using the Lattice Boltzmann Method (LBM) for aqueous Al_2O_3-based NFs through an etched glass micromodel. The research findings revealed that the small-sized Al_2O_3 NPs passed through the pore throat of the micro model without causing any blockage and change in permeability. The results also showed that 2D LBM simulations could be used in 3D micro models by replacing the viscous drag force in LBM equations. A reasonably good agreement was found in the experimental and numerical findings. In another study by Zarei et al. [24], a flow simulation approach in a nano-channel with a porous medium was carried out employing LBM. The results demonstrated that wall slip velocity and gas permeability were directly proportional to the Knudsen number. Moreover, the volume flow rate increased with porosity, and velocity increased with decreasing porosity. Permeability and Darcy coefficient decreased with ain increase in channel's average pressure. The thermal performance and dispersion stability of MWCNT-based NFs were studied by Azimy et al. [25] in a sono heat exchanging system. The heat exchanger integrated with an ultrasonic transducer showed improved/better thermal performance with improved dispersion stability of NFs. The HTC was reported to increase with concentration of NPs; however, at higher flow rates, the effect of ultra-sonication waves was not significant in HTC enhancement. For the experimental testing with and without incorporating the ultrasonic transducer, in the mass concentration of NPs 0.12–0.25%, the maximum enhancement in HTC was 96% and 77%, respectively, for a Reynolds number of 1753. The study confirmed that the simultaneous use of ultrasonic waves and NFs could enhance the HTC by up to 300%.

Wen et al. [26] studied the effect of NPs loading NPs (0.75–1.5 vol %), the flow rate of NFs (Re = 100–3750), and channel diameter (1.22–1.42 mm) on the thermal and hydraulic performance of the aqueous ZnO NFs. Results indicated that NFs showed superior thermal performance with smaller channels in a turbulent flow regime. For Reynolds numbers near 1400, the most significant enhancement of 52% in the HTC was observed for a channel diameter of 1.22 mm and at a 1.5% volume concentration of NPs. The corresponding maximum augmentation in friction factor was 11.7% at the Re of 2780. For the estimation of the Nusselt number with high accuracy, a new method based on Genetic Algorithm-optimized Backpropagation-Artificial Neural Network (GA-optimized BP-ANN) was developed. The model showed a maximum deviation of 2.70% from experimental investigation. In another similar kind of study with aqueous ZnO/EG-based NFs, Wen et al. [27] found an enhancement of 10.6 and 13.2% for the volume concentration of NPs 0.75 and 1.5%, respectively. The corresponding augmentation in the friction factor was 31.2% and 47.3% due to the intensification of the viscosity of the NFs. BP-ANN model predicted the Nusselt number and friction factor of NFs in the heat exchanging medium with a maximum deviation of 0.39% and 0.35%, respectively. Balla et al. [28] studied the thermal performance of ZnO/DIW NFs in free impingement jet and found thermal performance augmentation up to 133% compared with BFs for NPs concentrations of 0.1–0.5%.

Wen et al. [29] analyzed the heat transfer and flow behaviour of aqueous ZnO/EG NFs experimentally and using CFD simulations through two multiport mini tubes of the hydraulic diameter of 1.22 and 1.42 mm, respectively. For the volume concentration of NPs 0.75–1.50%, heat transfer augmentation was 6.7–9.8%, at the cost of increased frictional losses of 4.6–8.6%, respectively. The experimental findings showed that the HTC, pressure gradient and frictional losses increased with shrinking channel diameters. The single phase numerical model well predicted the Nusselt number and friction factor with a maximum deviation of 16.0% and 19.1%, respectively. Ahmad et al. [30] investigated the thermal conductivity and heat transfer performance of ZnO/DIW NFs in a square heat exchanger (length, 1.2 m and cross section 0.01 mm) at 0.025–0.1 wt% of NPs. At a temperature of 45 °C and 0.1 wt % loading of NPs, a significant enhancement of 52.0% in TC was recorded. The corresponding rise in the Nusselt number was recorded to be 47% at the end of the square pipe. In another study, Martínez et al. [31] examined the thermal characterization, and dispersion stability of aqueous ZnO NFs in microchannel heat sinks in a mass concentration of 1.0–3.0%. NFs were found stable up to 168 h for 1.0 wt % of NPs. Under the constant heat flux boundary conditions, 42.33% intensification in the HTC for the heat sink configurations was reported.

Although many experimental investigations studied the thermal and hydraulic features of metal oxide-based NFs in compact channels, only a few studies have been reported using aqueous-based ZnO NFs in compact channels. Hence, the present experimental

work aimed to examine thermal (heat transfer) and fluid flow (pressure drop) characteristics of ZnO/DIW based NFs in small diameter stainless steel test tubes (1.0–2.0 mm), keeping all other design parameters and operating conditions constant. Furthermore, the investigation was aimed to be conducted under constant heat flux and laminar flow (12–24 ml/min) conditions, for NPs loading varied within 0.012–0.048 wt%.

2. Materials and methods

2.1. NFs preparation setup

ZnO NPs (20 nm) were procured from Nanostructured & Amorphous Material, USA. The DIW was acquired locally. Ultra-sonication bath, magnetic stirrer, glass vials, beakers, and microbalance were utilized to synthesize NFs. The detailed specifications of the subject instruments can be traced from an earlier investigation [32] from the authors.

2.2. Preparation of NFs

One-step and two-step methods are commonly employed techniques for synthesising NFs. The present investigation used the two-step technique since it is simpler and more cost-effective than the one-step method [33]. First, the characteristic mass (12, 24, 36 and 48 mg) of the NPs was measured with a precise digital microbalance (AWU-220D, Shimadzu). After that, ZnO NPs were added to 100 ml DIW. Then, for uniform dispersion, the NFs were subjected to magnetic stirring (Heidolph MR Hei-End) for 1 h at 1000 rpm. Next, to further improve the dispersion stability of the prepared NFs, an ultra-sonication water bath (Elma E100H) was used for 3.0 h of sonication at 550 W, 240 V, and 50 Hz. Next, the NFs were subjected to 30 min of magnetic stirring and 30 min of ultrasonication to ensure enhanced dispersion stability. Finally, a fresh batch of NFs was used to record the results of each experimental test. The core characteristics of NPs and DIW are shown in Table 1.

3. Experimental setup and procedures

This section describes the experimental test setups used for stability, thermal conductivity (TC), viscosity (VC) and heat transfer coefficient (HTC) of the aqueous ZnO NFs under a range of designed operating conditions.

3.1. Dispersion stability of NFs

The stability of NFs is a growing concern, and researchers have used different techniques its proper investigation [34]. In this work, the visual photography technique assessed the dispersion stability by measuring the transparent section of the NFs at the top of the glass vials over the investigated time. First, the glass vial was divided into equal sections by placing a precise scale across it, and then the transparent section of the fluid was measured with great care to determine the NP's settling rate. The method is easy and widely used to find the stability of NFs, as reported in the literature [35]. Different snapshots were captured at regular intervals with the help of a high resolution and magnification digital camera. Then the recorded snapshots were compared to assess the NFs' stability [36].

3.2. Thermal conductivity of NFs

ZnO NFs were tested for their TC using a Transient Hot-Wire technique [37]. The TC was investigated in the given mass concentration of NPs in the 20–60 $^{\circ}$C temperature range. A digital thermal conductivity analyzer (TEMPOS, METER GROUP, USA) was used in this study. This thermal analyzer comprises of KS-3 needle sensor and microcontroller. KS-3 needle sensor was connected to the microcontroller with a data cable. This needle sensor can measure the TC up to 2.0 W/mK. To ensure the accuracy of the analyzer, it was calibrated by testing the TC of the standard glycerin sample within± 1.0% uncertainty. The desired temperature of NFs was maintained using a thermal bath (TC-550MX, USA). The data was collected for steady-state operating conditions. The test setup was validated by comparing the measured data with the NIST database [38], and the deviation of the experimental findings from those obtained from the NIST database was within ±1.0%, as presented in Table 2.

3.3. Viscosity of NFs

The viscosity (VC) of the fluid is a prerequisite for estimation of pressure drop and related frictional losses within the heat exchanging systems [39]. In the current study, the VC of NFs was studied in 20–60 °C temperature range using a Rotary Rehometer having an S1 rotor under varying shear rates (0.01–1000 s^{-1}). A standard data acquisition software (RHEOTEST RN 5.1) was used to extract the measured data. The test setup was validated by comparing the measured data (collected with DIW) with the NIST database [38]. The deviation between the experimental and theoretical findings obtained from the NIST database was within ±1.0%, as presented in Table 2.

Table 1
Thermal and physical characteristics of ZnO NPs and DIW at 20 °C

Property (−)	Density, ρ (kg/m^3)	Thermal conductivity, k (W/m.K)	Specific heat capacity, C_p (J/kg.k)	Average diameter (nm)
ZnO	5600	29.0	514	20
DIW	998	0.598	4184	-

Table 2
Validation of experimental setup for TC and VC measurement of NFs

Thermophysical properties	Temperature (°C)	Experimental data	NIST database	Deviation (%)
Thermal conductivity (mW/m.K)	20	604.7	598.4	1.05%
	30	619.4	615.5	0.63%
	40	632.5	630.6	0.30%
	50	644.0	643.5	0.07%
	60	654.0	654.3	−0.04%
Viscosity (mPs.s)	20	1.002	1.001	0.09%
	30	0.797	0.797	0.00%
	40	0.645	0.652	−1.08%
	50	0.541	0.546	−0.91%
	60	0.464	0.466	−0.42%

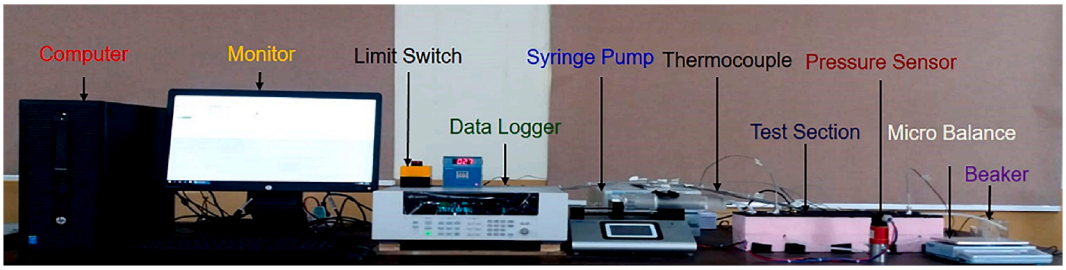

Fig. 1. Experimental setup for thermal and hydraulic characteristics of NFs.

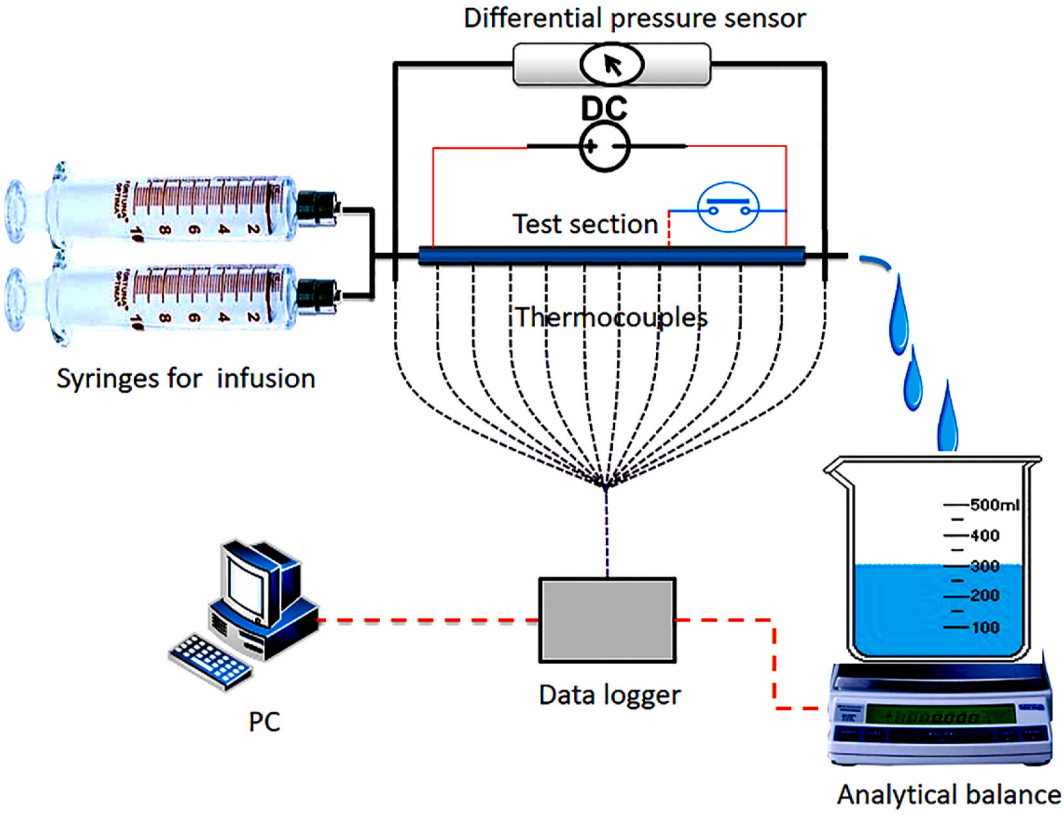

Fig. 2. Schematic diagram of the experimental test setup for thermal and hydraulic characteristics of NFs.

3.4. Thermal performance of NFs

The experimental setup and its schematic diagram for heat transfer performance are shown in Figs. 1 and 2. The test set-up comprises three mini-channel stainless steel tubes with inside diameters of 1.0 mm, 1.5 mm and 2.0 mm and each with characteristics axial length of 330 mm. The wall thickness of each tube was 0.5 mm. NFs samples were injected into the test section using a highly precise dual syringe pump (Legato 200 KDS) to maintain a constant flow rate. The syringe pump used two glass syringes 120 ml each to maintain the desired flow rate.

All the experiments were performed in a laminar flow regime (12–24 ml/min). The flow rate was also cross-checked with the help of microbalance. The stainless steel test section was subjected to constant heat flux using a DC power supply (LONG WEI, LW3060KD). The fluid temperature at the inlet and outlet and outer wall surface temperature of the test section was measured with K-type thermocouples. Overall twelve thermocouples were used for the temperature meaurement. All thermocouples were calibrated in the reference thermal bath within a 10-70°C temperature range. To ensure the proper thermal conduction to the thermocouples from the outer surface of the wall, all thermocouples were attached using a highly thermally conductive and electrically insulating epoxy (Omega OB-101-1/2). Fibreglass insulation was used to isolate the test setup from the environmental effects. In addition, a pressure transducer (Huba Control 692, 0–1 bar) was installed across the mini tube test setup (inlet and outlet) to investigate the pressure gradient of the NFs. A data logger (Keysight 34970A) was used for recording the data. The data was collected under steady-state operating conditions to estimate the average and local HTCs and the pressure and frictional losses within the test section.

3.5. Data analysis for NFs

The volume concentration against the mass concentration of the NPs within the prepared NFs has been estimated using the correlation presented in Eq. (1) [40]. Here, φ, ρ_{bf}, ρ_{np}, ρ_{nf}, W_{np} and W_{bf} are the volume concentration of NPs, density of DIW, density of NPs, density of the NFs, the mass of NPs, and the mass of BFs, respectively.

$$\varphi = \frac{W_{np} \times \rho_{bf}}{\left[\rho_{np}\left(1 - W_{np}\right) + W_{np} \times \rho_{bf}\right]} \tag{1}$$

The density (ρ_{nf}) and specific heat capacity (Cp_{nf}) of the NFs are the prerequisites for evaluating their heat transfer potential and can be found using the two-phase mixture theory as presented in Eqs. (2) and (3) [41,42], respectively.

$$\rho_{nf} = (1 - \varphi)\rho_{bf} + \varphi \times \rho_{np} \tag{2}$$

$$C_{p_{nf}} = \frac{\varphi\rho_{np}C_{p_{np}} + (1 - \varphi)\rho_{bf}C_{p_{bf}}}{\rho_{nf}} \tag{3}$$

The Cp_{np}, Cp_{nf} and Cp_{bf} are the specific heat capacities of NPs, NFs and DIW. The convective HTC of the NFs was measured using correlation as presented in Eq. (4) [43].

$$h_x = \frac{q''}{T_{iw(x)} - T_{f(x)}} \tag{4}$$

where $q^{"}$, $T_{iw(x)}$, $T_{f(x)}$, and $h(x)$ are the applied heat flux, inner wall and bulk fluid temperatures and the HTC in the axial direction of the minichannel test setup. The subject parameters can be estimated using the correlations as presented Eqs. (5)–(7), respectively.

$$q'' = \frac{Q}{A} \tag{5}$$

Q is the applied input power to the mini tube and can be estimated using correlation Q = VI. A is the surface area of the tube and can be estimated using the correlation ($A = \pi.Di.L$).

$$T_{w(x)} = T_{os} - \frac{Q.ln\left(\frac{D_o}{D_i}\right)}{2.\pi.L.K_{tube}} \tag{6}$$

$$T_{f(x)} = T_{in} + \frac{q''.\pi.D_i.X}{\dot{m}.C_{p_{nf}}} \tag{7}$$

where T_{os} is the wall outer wall surface temperature, Di and Do are the inner and outer diameters of the test section. K_{tube} is the TC of the tube material, ṁ is the mass flow rate, and x is the horizontal length of the tube from the leading edge. L is the total length of the test section. The Nusselt number (Nu) is calculated using Eq. (8) [44]. The Reynolds (Re) number of the NFs was determined using Eq. (9) [45]. Here ρ, ν, D and μ are the density, kinematic and dynamic viscosities of the NFs, while D_i is the inner diameter of the test section.

$$Nu = \frac{h.D_i}{K_{nf}} \tag{8}$$

$$Re = \frac{\rho_{nf} \times v_m \times D_i}{\mu_{nf}} \tag{9}$$

Shah's correlation is usually used to compute the local *Nu* as a function of the Graetz number (Gz) in the test section subject to the constant heat flux when the fluid flow is in a laminar regime. The governing equation used to compute the *Nu* is shown in Eq. (10) [8].

$$Nu_x = \begin{Bmatrix} 1.302 \cdot x_*^{-1/3} - 1 & x_* \le 0.00005 \\ 1.302 \cdot x_*^{-1/3} - 0,5 & 0.00005 \le x_* \le 0.0015 \\ 4.364 + 8.68 \cdot \left(10^3 \cdot x_*\right)^{-0,506} \cdot e^{-41 \cdot x_*} & x_* \ge 0.0015 \end{Bmatrix} \tag{10}$$

where x* is the reciprocal of Gz, representing the distance along the axis of the test section as presented in Eq. (11) [8].

$$x^* = [(x / d) / (Re \cdot Pr)] \tag{11}$$

The average HTC can be determined at the entrance region of the test section at uniform heat flux and laminar flow conditions using Eq. (12) [8].

$$Nu_{avg} = \begin{cases} 1.953(Re.Pr.D/L)^{(1/3)} & (Re.Pr.D/L) \ge 33.3 \\ 4.364 + 0.0722.(Re.Pr.D/L) & (Re.Pr.D/L) < 33.3 \end{cases} \tag{12}$$

Besides that, the friction factor is measured using Darcy correlation under laminar fluid flow and can be calculated using the correlation shown in Eq. (13) [15].

$$f = \frac{64}{Re} \tag{13}$$

3.6. Uncertainty analysis

Uncertainty in reported results is of acute importance as it determines quality of repeatability for any experimental results. Various variables' uncertainties determine the parameter's uncertainty which is a function of the sum of these factors. For example, consider z as a function of various independent variables, Xi, each having its level of uncertainty, ΔXi, the total level of uncertainty in z, can be estimated with Eq. (14).

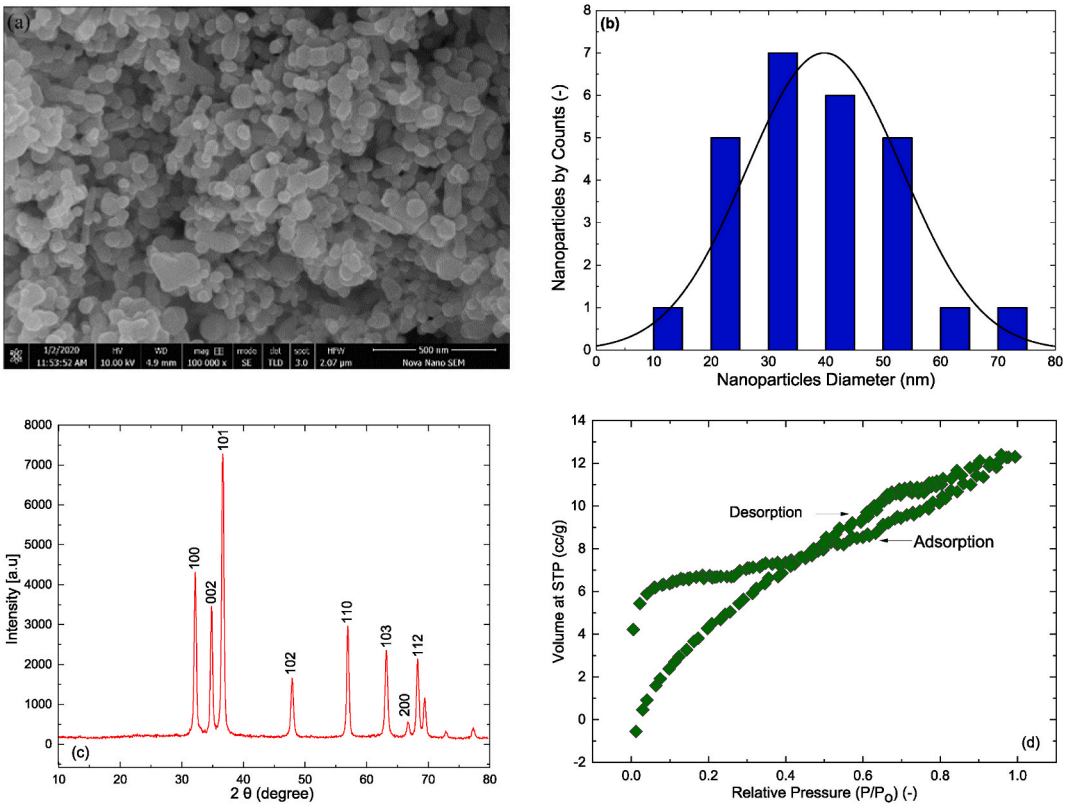

Fig. 3. ZnO NPs (a) SEM image at 100,000 magnification (b) Average size distribuatation (c) XRD spectrum (d) Adsorption-desorption isotherms.

$$\Delta z = \pm \sqrt{\sum_{i=1}^{n} \left(\frac{\partial f}{\partial Xi}\right)^2 (\Delta xi)^2} \tag{14}$$

The uncertainties in the independent parameters such as axial length of the mini tube, the diameter of the mini tube, temperature and pressure gradient were ±1.0 mm, ± 0.01 mm, ± 0.1°C, and 1.25%, respectively, while the uncertainties in the mass flow rate, TC, VC, density, specific heat capacity, were 1.0% of the recorded experimental values. The corresponding uncertainties in the dependent parameters, such as in surface area (A_s), friction factor (f), pumping power (P), fluids velocity (u), Reynolds number (Re), local HTC (h_{local}), average HTC (h_{avg}), local *Nu* (Nu_{local}) and average *Nu* (Nu_{avg}), 1.04%, 5.25%, 1.89%, 2.45%, 1.73%, 5.15%, 3.60%, 5.34%, and 4.20%, respectively.

4. Characterization of NPs

4.1. SEM analysis of NPs

The NP's morphological characteristics and size are commonly measured using Scanning Electron Microscopy (SEM) [46]. The present study investigated the morphology and primary particle size of NPs using SEM (Nova Nano 450). Fig. 3 (a) shows the processed image of SEM at 100,000 magnification. The size distribution found by processing the SEM image in Image J software, as shown in Fig. 3 (b), was at about 33 nm.

4.2. XRD analysis of NPs

X-ray diffraction (XRD) is the widely accepted technique for investigating the crystalline behaviour of any NPs [47]. This study determined the crystalline behaviour of ZnO NPs using Bruker D2-Phaser Germany Model-D2 XRD, as shown in Fig. 3 (c). XRD peaks were recorded in the 10°-80° range. Fig. 3 (c) presents the different peaks of the XRD pattern, which were found at 31.737°, 34.379°, 36.215°, 47.484°, 56.536°, 62.777°, 66.304°, 67.868°,69.009°. Comparatively miller indices value was (100), (002), (101), (102), (110), (103), (200), (112). The XRD pattern confirms the monoclinic crystalline structure of ZnO particles with lattice constants of (a = b = 3.2530 A° c = 5.2130A°). These indexed well match those in (Joint Committee on Powder Diffraction Standards, i.e. JCPDS card number 036–1451) [48]. Besides that, it also showed the highest purity of the NPs. The diameter of ZnO NPs was measured using Debye- Scherrer Eq. (15).

$$d = 0.89\lambda / (\beta * \mathrm{Cos}\,\theta) \tag{15}$$

In Eq (13), Scherrer constant = 0.89, λ, θ, and β are the X-rays wavelength, Bragg's diffraction angle, and full width at half maximum (FWHM) diffraction peak and are measured in radians. The average diameter of NPs was nearly 18.53 nm, as determined using Eq. (13).

4.3. BET analysis of NPs

NPs' pore size, specific area, and pore volume significantly affect heat transfer rate for better thermal application. Hence, it is crucial to find the vent size and pore volume of the NPs. Brunauer-Emmett-Teller (BET) technique is the broadly employed methodology for finding the specific surface area (SSA) of NPs [49]. In this method, the subject characteristics of NPs are estimated by adsorption and desorption of nitrogen gas. The volume flow technique can determine the temperature of the nitrogen in the liquid state and the magnitude of the adsorbed gas [50]. The current research investigation determined the SSA of NPs by using the NOVA 3200e surface area analyzer. For the first 5.0 h, the sample (150 mg) was held at 100°C to eliminate any unwanted impurities. Then the specific surface area is then analyzed based on adsorption-desorption isotherms data. The isothermal curve of adsorption and desorption is shown in Fig. 3 (d). The surface area was determined to be about 22.37 m^2/g. However, the specific surface area was less than described by the manufacturer, and the possible reason might be due to the agglomeration of NPs over time.

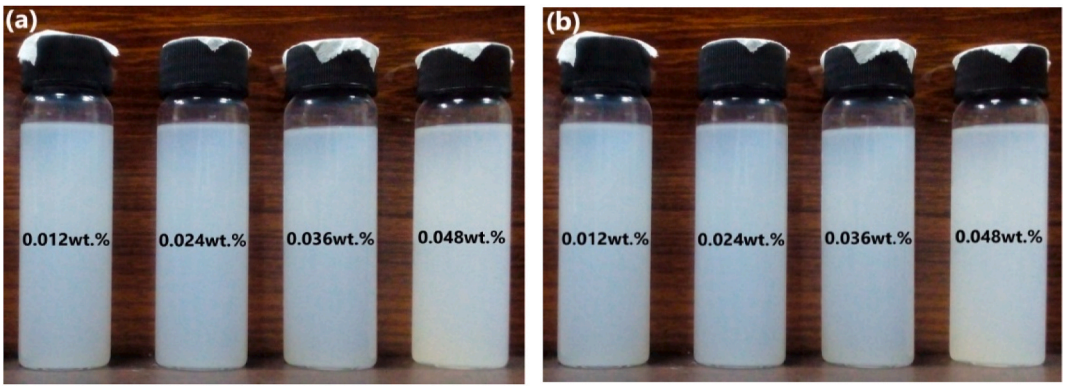

Fig. 4. (a) ZnO/H_2O NFs right after preparation (b) right after 48 h.

5. Results and discussions

5.1. Dispersion stability of NFs

The stability of the prepared NFs was assessed by the visual photography method by measuring the transparent section of the NFs at the top of the glass vials over the investigated time. Fig. 4 (a) and 4 (b) display the visual inspection of the samples immediately after formulation and after 24 h.

The inspection showed no sign of sedimentation after 24 h without adding any surfactant. The possible reason is the low agglomeration of NPs under the optimized time of intensive ultrasonication followed by magnetic stirring. Another reason is the presence of strong electrostatic repulsion forces between the NPs because of the smaller size of the NPs. The findings of the present investigation conform with the study conducted with ZnO/DIW-based NFs [31]. Furthermore, the research results showed the dispersion stability of the prepared NFs was enough for their application in mini tube heat exchanging systems without any significant fear of agglomeration and particle deposition on the inner surface of the channel.

5.2. Thermal conductivity NFs

An increasing trend has been observed in the TC of DIW and all prepared NFs with the rise in temperature and NPs loading, as presented in Fig. 5 (a). The behaviour observed was consistent with another study conducted with aqueous-based ZnO NFs [51]. The recorded uncertainty in the measured experimental results was ±1.0%. From Fig. 5 (a), the increase in TC was observed up to 3.81% at 0.012 wt %, 8.96% at 0.024 wt %, 13.70% at 0.036 wt % and 18.27% at 0.048 wt % of NPs compared to DIW at 40 °C. The possible enhancement in NFs thermal conductivity is due to ZnO NPs concentration in the host BFs and increased Brownian motion of NPs with temperature. Another reason is the interfacial layer between the ZnO NPs and the host BFs, which enhances the thermal performance of the NFs [52]. The findings were compared with the well-known empirical models from the published literature, as presented in Table 3. However, the results shown in Fig. 5 (c) indicated that the classical correlations failed to estimate the experimental TC of the NFs. The possible reason could be different operating conditions, mass concentrations of NPs, and the size and morphology of NPs considered for modelling these correlations.

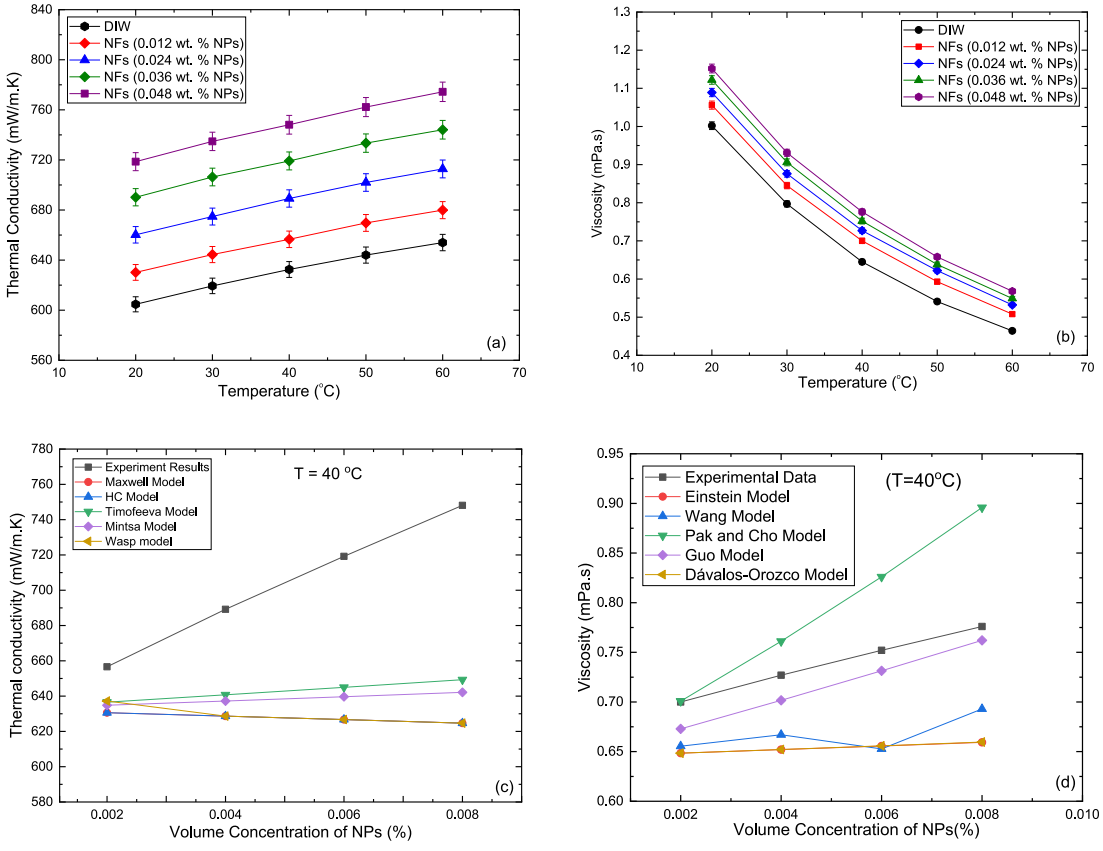

Fig. 5. ZnO/DIW NFs (a) thermal conductivity and (b) viscosity as a function of temperature and NPs loading (c) thermal conductivity and (d) viscosity, comparison with classical correlations.

Table 3
Classical models for the evaluation of TC of NFs

Thermal Conductivity Model	Mathematical expression	Results Deviation (%)
Maxwell model [53]	$\frac{k_{eff}}{k_f} = \left[\frac{k_p + 2k_f + 2\Phi(k_f - k_p)}{k_p + 2k_f - 2\Phi(k_f - k_p)}\right]$	12.00
Hamilton and Crosser [54]	$\frac{k_{eff}}{k_f} = \left[\frac{k_p + (n-1)k_f - (n-1)\Phi(k_f - k_p)}{k_p + (n-1)k_f + \Phi(k_f - k_p)}\right]$	12.00
Timofeeva Model [55]	$\frac{k_{eff}}{k_f} = (1 + 3\varphi)$	9.30
Wasp model [56]	$\frac{k_{eff}}{k_f} = \left[\frac{k_p + 2k_f - 2\Phi(k_f - k_p)}{k_p + 2k_f + 2\Phi(k_f - k_p)}\right]$	11.70
Mintsa et al. [57]	$\frac{k_{eff}}{k_f} = (1 + 1.72\varphi)$	10.10

5.3. Viscosity of NFs

The VC of DIW and NFs samples has been measured for varying concentrations of NPs (0.012–0.048 wt %) and operating temperatures (20–60 °C) using a rotary rheometer. The analytical findings presented a strong dependency of the NFs' viscosity on the NP's loading and operating temperature. The viscosity was directly related to the NP's loading while inversely proportional to the temperature of NFs. The behaviour observed was consistent with another study conducted with aqueous-based ZnO NFs [51]. The uncertainty in the measured results is ±1.0%. Fig. 5 (b) shows that the percentage rise in VC for ZnO/DIW-based NFs was observed up to 8.52% at 0.012 wt %, 12.71% at 0.024 wt %,16.58% at 0.036 wt % and 20.31% at 0.048 wt % mass concentrations of NPs compared to DIW at 40 °C. The viscosity rise with a concentration of NPs attributes to the fact that the interfacial forces between the adjacent layers of the NFs increased with the increase in NPs loading. The same fact is attributed to the effect observed with the decrease in NFs temperature and vice versa.

The analytical results were compared with the well-known theoretical models from the existing literature, as presented in Table 4. The results shown in Fig. 5 (d) indicated that the theoretical models failed to estimate the experimental TC of the NFs. The possible reason could be different operating conditions, mass concentrations of NPs, and the size and morphology of NPs considered for modelling these correlations.

5.4. Validation of experimental setup

The test setup's reliability and accuracy were validated by comparing the experimental values of DIW calculated for the Nusselt number and the friction factor with those predicted by the well-known theoretical models. The comparative analysis for all three tube diameters has been presented in Fig. 6 (a) and (b) at 12–24 ml/min flow rates. The findings showed a good agreement between the experimental and theoretical results for the average Nusselt number and friction factor predicted by the Shah correlation [62] and the famous Darcy Correlation [63]. The maximum deviation between experimental and theoretical results was within ±5.86% and ±2.80% for Nusselt number and friction factor, respectively.

5.5. Local heat transfer coefficient of NFs

Fig. 7(a–f) show the local HTC variance along the axial length of the test section at different flow rates and diameters of the tube for DIW and 0.048 wt % NPs of ZnO NFs. The literature surge also revealed a similar kind of behaviour of aqueous ZnO NFs in the compact channel heat exchangers [26]. The experiments were performed with tubes with 1.0, 1.5, and 2.0 mm inside diameters and varying flow rates in the 12–24 ml/min range. The results indicated that the local HTC values at the tube's entrance region were high and gradually fell along the tube's axis. The possible reason for high HTC at the test section entry region is that the flow is not fully developed. At the same time, across the test section length, the HTC reduces as soon as the flow becomes fully developed, leading to a constant HTC value.

It can also be observed that the HTC increased with NPs loading and fluid flow rate compared to DIW. The increment in local HTC values is due to the high TC of ZnO NFs compared to DIW. In addition to fore-stated observation, it is evident that the local HTC values possessed an inverse proportion with diameter of the test section. This is because an increase in tube diameter will decelerate the flow (at fixed flow rate), reduce the Reynolds number, and hence the HTC. The Brownian motion of NPs could be plausible cause for the stated trends at low velocity within large tube. The maximum rise of local HTC is 17.11% compared with DIW, which is observed at

Table 4
Classical models for the viscosity prediction of NFs

Viscosity Model	Mathematical expression	Results Deviation (%)
Einstein's model [58]	$\mu_{nf} = (1 + 2.5\varphi)\mu_f$	12.90
Wang model [59]	$\mu_{eff} = \mu_f(1 + 7.3\varphi + 123\varphi^2)$	10.70
Pak and Cho model [60]	$\mu_{nf} = (1 + 39.11\varphi - 533.9\varphi^2)\mu_f$	6.70
Guo et al. [12]	$\mu_{eff} = \mu_f(1 + 2.5\varphi + 6.5\varphi^2)(1 + 350\varphi/d_p)$	3.0
Dávalos-Orozco [61]	$\mu_{eff} = \mu_f(1 + 2.5\varphi + 6.17\varphi^2)$	12.90

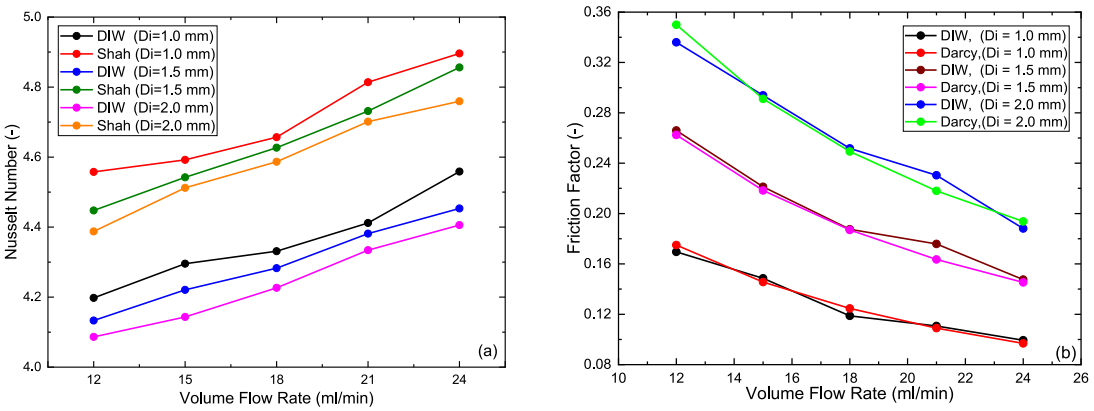

Fig. 6. Comparison of DIW experimental and theoretical results for (a) Nusselt Number vs volume flow rate (b) Friction Factor vs volume flow rate.

24.0 ml/min when the tube's diameter is 1.0 mm. Under similar operating conditions, this rise was 14.82% and 11.61% for 1.5 mm and 2.0 mm diameter test sections, respectively.

Experimental findings of the local HTC were compared with the predictions obtained by Shah Correlation, as shown in Fig. 8 (a) and (b) for the 0.012 wt % and 0.048 wt % loading of NPs. The result showed that most of experimental datapoints for ZnO/DIW NFs were in ±10% deviation from Shah Correlation. The deviation of the analytical results from the predicted results attributes to the optimized and standard operating conditions, the ideal temperature and velocity distribution within the NFs, and the uniformly developed velocity and thermal boundary layers, which could be compromised to some extent in the practical case.

5.6. *Average heat transfer coefficient of NFs*

Fig. 9(a–c) shows the experimental results of the average HTC plotted against volume flow rates for DIW and ZnO NFs for different tube diameters. The literature surge also revealed a similar kind of behaviour of aqueous ZnO NFs in the compact channel heat exchangers [26]. It is observed from the analytical findings that the average HTC increases/improves/enhances with the volume flow rate and the NPs concentration in the BFs; however, an increase in tube diameter has inversely affected the HTC due to a decrease in the Reynolds number at the same flow rate. This augmentation in average HTC is due to the increased loading of ZnO NPs in the BFs. Another reason for enhancing heat transfer is the Brownian movement of NPs at higher Reynold numbers. The maximum rise in the average HTC was 13.05% compared with DIW, at 0.048 wt % of NPs when the tube's diameter was 1.0 mm at a 24.0 ml/min fluid flow rate. This enhancement was observed to be 12.14% and 9.79% for the tubes with 1.5 mm and 2.0 mm diameters. Similar reasons exist for this variation in average HTC with the change in tube diameters, as observed in the case of local HTC. The results presented in Fig. 9 (d) showed that most of the findings for ZnO/DIW NFs were in the range of ±10% deviation compared to Shah Correlation.

5.7. *Friction factor of NFs*

Fig. 10 represents the variations in friction factor (*f*) against volume flow rate at different mass concentrations of ZnO NPs. The analytical findings showed that the friction factor decreased as the volume flow rate increased. It is also evident from the experimental findings that the effect of NPs loading on the friction factor at low volume flow rates of NFs was more significant. The friction factor increased with NPs charging in pure fluid at a lower volume flow rate. At low flow rates, the viscous forces are dominated by inertia forces. Haghighi et al. [64] observed similar behaviour in their study of different metal oxide-based NFs in an aqueous media.

Therefore, adding the NPs in DIW increases shear stress among the layers and friction increases. The maximum friction factor obtained was about 28.85%, 19.25% and 12.72% for 1.0 mm, 1.5 mm and 2.0 mm diameter tubes, respectively, at 0.048 wt % of NPs and at 12.0 ml/min fluid flow rate compared to DIW. The Reynolds number decreased with an increase in the test section diameter; hence it was attributed to lower shear stress and, consequently, the less viscous forces to the fluid flow. This indirectly shows the decrease in friction factor of the NFs with the decrease in Reynolds number of the NFs with an increase in channel cross-sectional diameter. It also shows that the friction factor was inverse to the tube diameter. At low flow rates, the viscous forces are dominated by inertia forces. Therefore, adding the NPs in DIW increases shear stress among the layers, and frictional losses increase. However, when the cross-sectional area increases, the velocity of the fluid decreases, and hence the viscous forces do not dominate the inertia forces. Therefore, the shear forces become weak within the tubes, and the friction factor decreases. Analytical findings were compared with predicted results by Darcy correlation for laminar flow, as shown in Fig. 10 (d). The result shows that predicted results obtained by the Darcy formula of friction factor for ZnO/DIW NFs were in good agreement with analytical findings in the ±8.0% deviation range.

5.8. *Pressure drop of NFs*

Fig. 11(a–c) represents the change in pressure gradient against volume flow rate for different diameters of tubes. As shown in Fig. 11, for both DIW and ZnO NFs, the pressure gradient increased with the volume flow rate and NPs loading but decreased with an

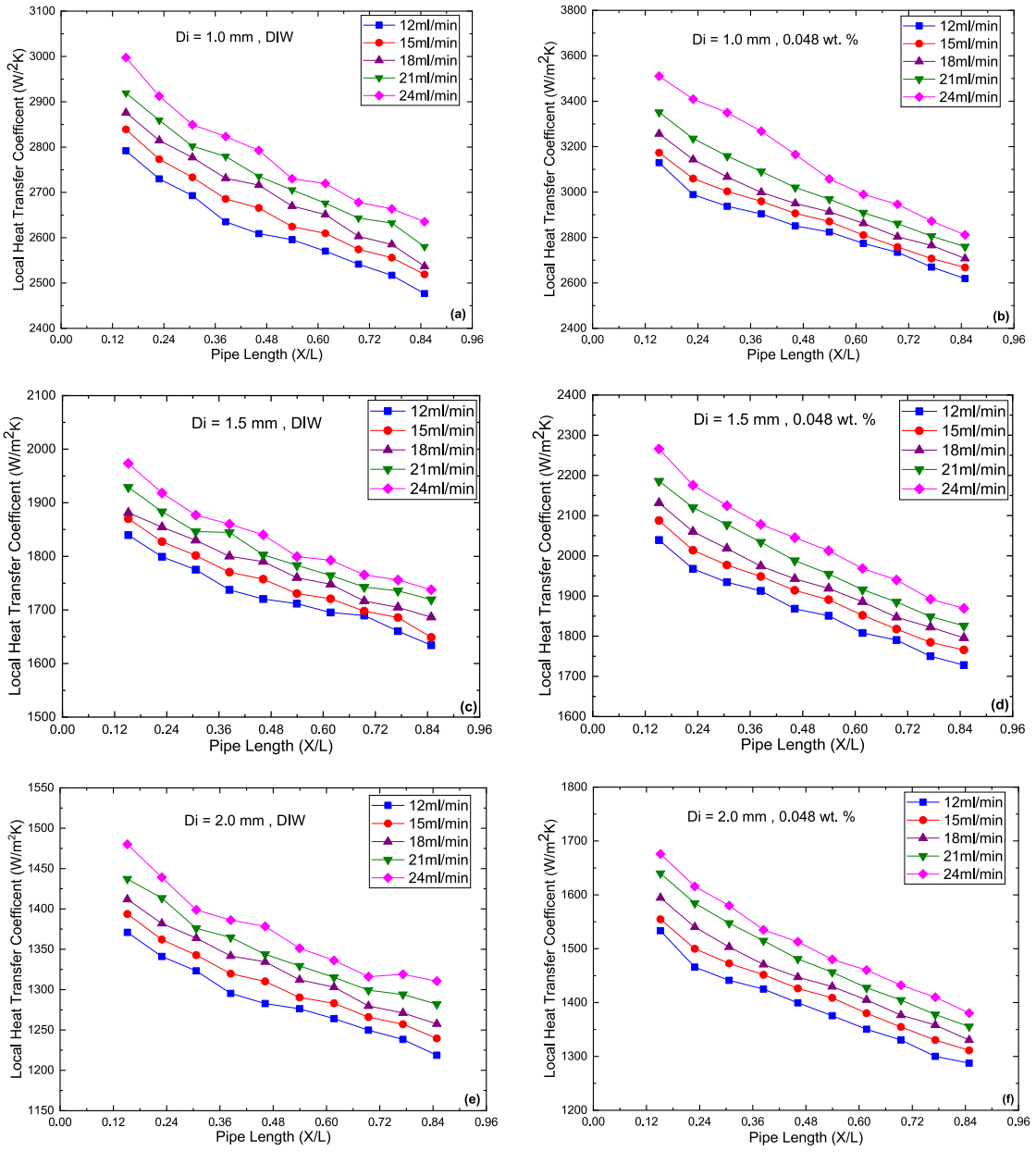

Fig. 7. Variations in local HTC of BFs and NFs for 0.048 wt % (a) DIW, Di = 1.0 mm (b) NFs, Di = 1.0 mm (c) DIW, Di = 1.5 mm (d) NFs, Di = 1.5 mm (e) DIW, Di = 2.0 mm (f) NFs, Di = 2.0 mm.

increase in tube diameter.

This is because viscosity increases with ZnO NPs loading in pure DIW, and the frictional losses increases. The maximum pressure drop is achieved up to 29.19%, %, 19.21%, and 12.25% for ZnO/DIW NFs with 1.0 mm,1.5 mm and 2.0 mm diameters of the tube at 0.048 wt % of NPs concentrations, respectively, compared to DIW. Haghighi et al. [64] observed similar behaviour in their study of different metal oxide-based NFs in an aqueous media.

Results proved that when the test section's diameters reduced, the change in pressure increased and vice versa. The cause is with the decrease in the diameter, the cross-sectional area reduces and the force per unit area increases, resulting in more pressure and vice versa. Experimental results were compared with predicted results by Darcy correlation, as shown in Fig. 11 (d). The result showed a good agreement between the analytical and theoretical findings within the ±5.0% deviation range. The deviation of the experimental results from the predicted results attributes to the optimized and standard operating conditions, the uniformly developed velocity and thermal boundary layers within the test section, which could be compromised to some extent in the practical case.

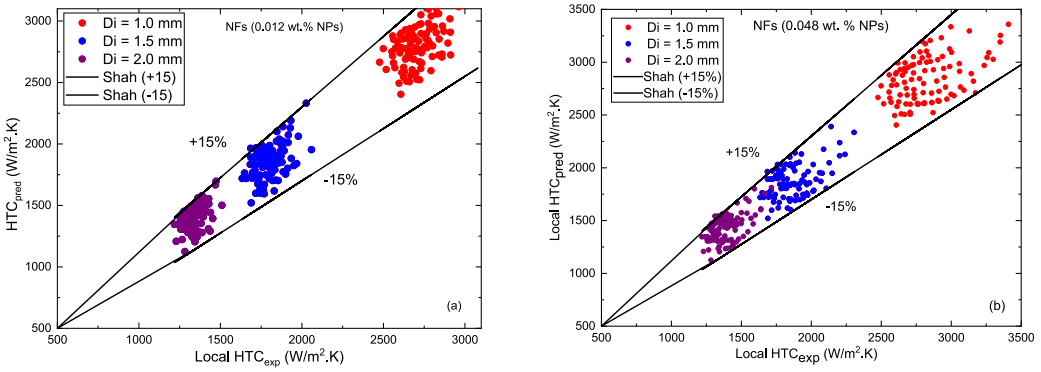

Fig. 8. Comparison of local HTC from Shah correlation prediction with experimental results for NFs in tubes of different diameters and NPs concentrations (a) at 0.012 wt % (b) at 0.048 wt %.

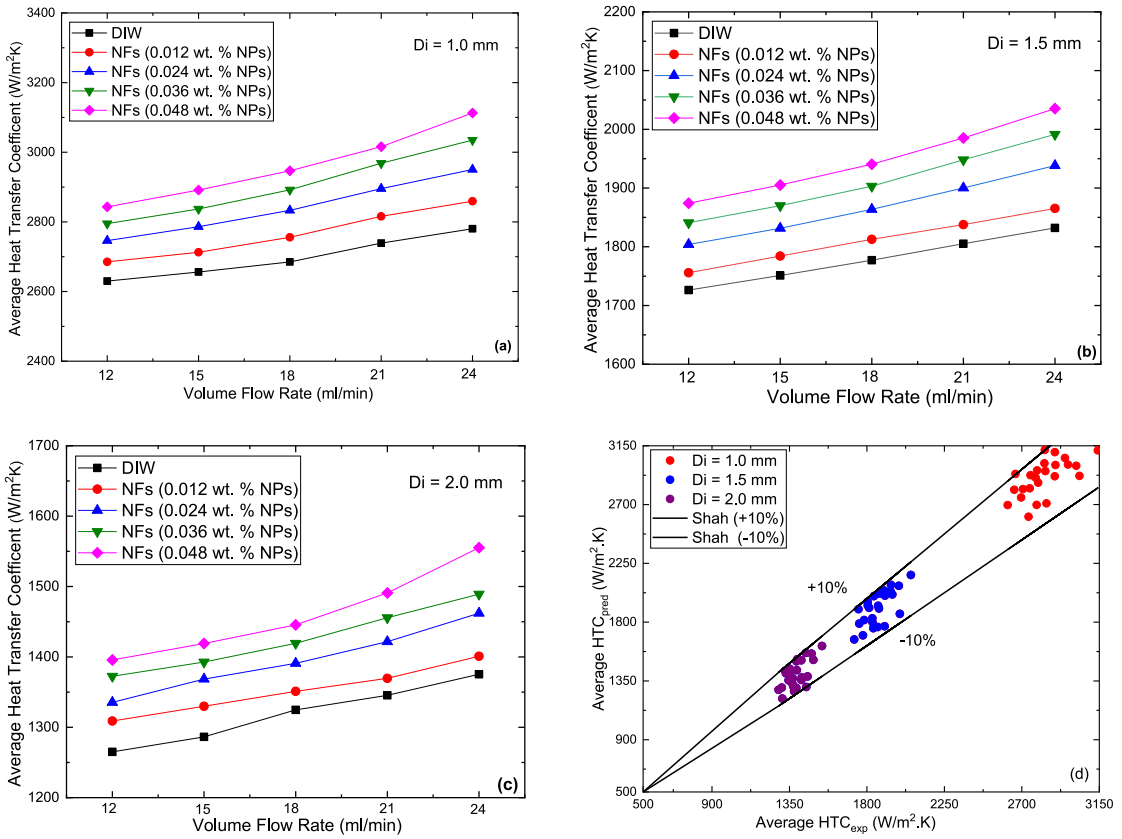

Fig. 9. Average HTC of ZnO-DIW as the function of volume flow rate (a) Di = 1.0 mm (b) Di = 1.5 mm (c) Di = 2.0 mm (d) Comparison with Shah correlation for NFs at 0.048 wt %.

6. Conclusion and future recommendations

Thermal and hydraulic performance of aqueous-based ZnO NFs with 0.012–0.048 wt % of NPs were investigated in small horizontal circular tubes of different inside diameters (1.0–2.0 mm) under laminar flow (12–24 ml/min) and constant heat flux boundary conditions. Besides that, in this study, different techniques for material characterization, such as XRD, BET analysis, and SEM, were used. The experimental findings result in the following conclusions.

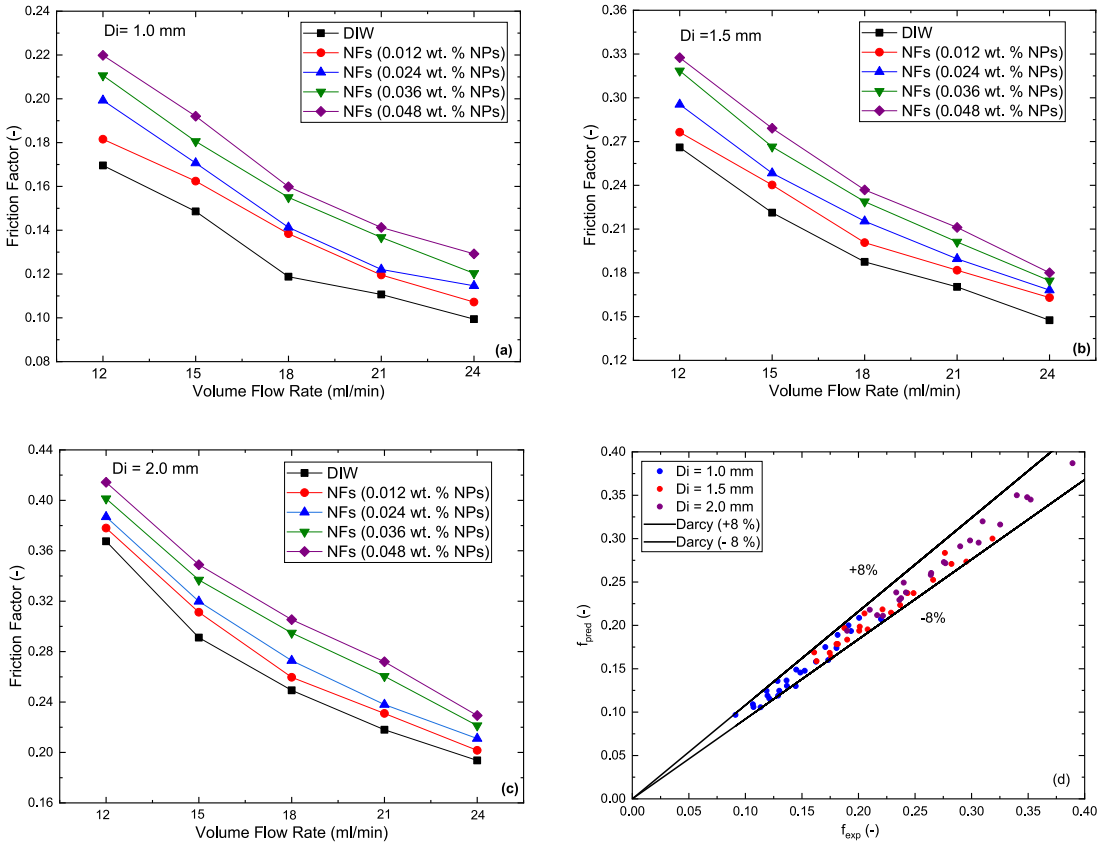

Fig. 10. Friction factor of ZnO-DIW as the function of volume flow rate (a) Di = 1.0 mm (b) Di = 1.5 mm (c) Di = 2.0 mm (d) Comparison with Darcy correlation for NFs at 0.048%.

1. It was observed from the experimental results that the TC of the NFs possessed a direct relation with the NPs loading and NFs temperature. In contrast, the VC was directly proportional to the NP's loading and had an inverse relation with the temperature. The maximum rise in TC and VC was observed up to 3.81%–18.27% and 8.52%–20.31%, respectively, at 40 °C for 0.012–0.048 wt % of NPs, respectively.
2. Local HTC and Nusselt's number intensified with the fluid flow rate and NPs mass concentration in the BFs but decreased with the rise in tube diameter. The maximum intensification in local HTC along the axial length of the tube was observed up to 17.11% compared with DIW, at 24.0 ml/min when the tube's diameter was 1.0 mm. The result showed that most experimental values were within the range of ±15% deviation compared to Shah Correlation. The average HTC and Nusselt's number also directly correlated with the fluid flow rate and NPs mass concentration in the BFs but decreased by increasing the tube diameter. For instance, the maximum average HTC growth was about 1.83% at 0.012 wt %, 6.12% at 0.024 wt %, 9.16% at 0.036 wt % and 13.05% at 0.048 wt % for 24 ml/min volume flow rate when tube diameter was 1.0 mm compared to DIW. An increase in tube diameter has inversely affected the fluid velocity, Reynolds number, and hence the HTC.
3. NFs have a more significant friction factor than DIW, increasing with NPs concentration in the host fluid and decreasing with the rise in volume flow rate. At a 12.0 ml/min flow rate, friction factor was observed up to 28.39% at 0.048 wt% for a 1.0 mm diameter of the tube. The friction factor reduced with the rise in tube diameter and vice versa. Analytical findings agreed with those obtained from the Darcy correlation within the ±8.0% deviation range. The Reynolds number decreased with an increase in the test section diameter; hence it was attributed to lower shear stress and, consequently, the less viscous forces to the fluid flow.
4. The maximum pressure drop was up to 29.19%, 19.21%, and 12.25% for ZnO/DIW NFs for 1.0 mm, 1.5 mm and 2.0 mm of tube diameters at 0.012 wt %, 0.024 wt %, and 0.036 wt % and 0.048 wt % of NPs, respectively, compared to DIW. Results proved that when the tube diameters were reduced in the test section, the change in pressure gradient increased and vice versa. The change in inner tube diameter affects the Reynolds number and the NFs velocity profile within the test section and hence the pressure gradient.

The research findings showed that at lower test section diameter, the local and average HTCs possessed enhanced values at the cost of more frictional and pressure losses due to interdependence of the Reynolds number on the cross-sectional area of the tube. However, with the rise in tube diameter and under similar operating conditions, a decrement was observed in the local and average HTC.

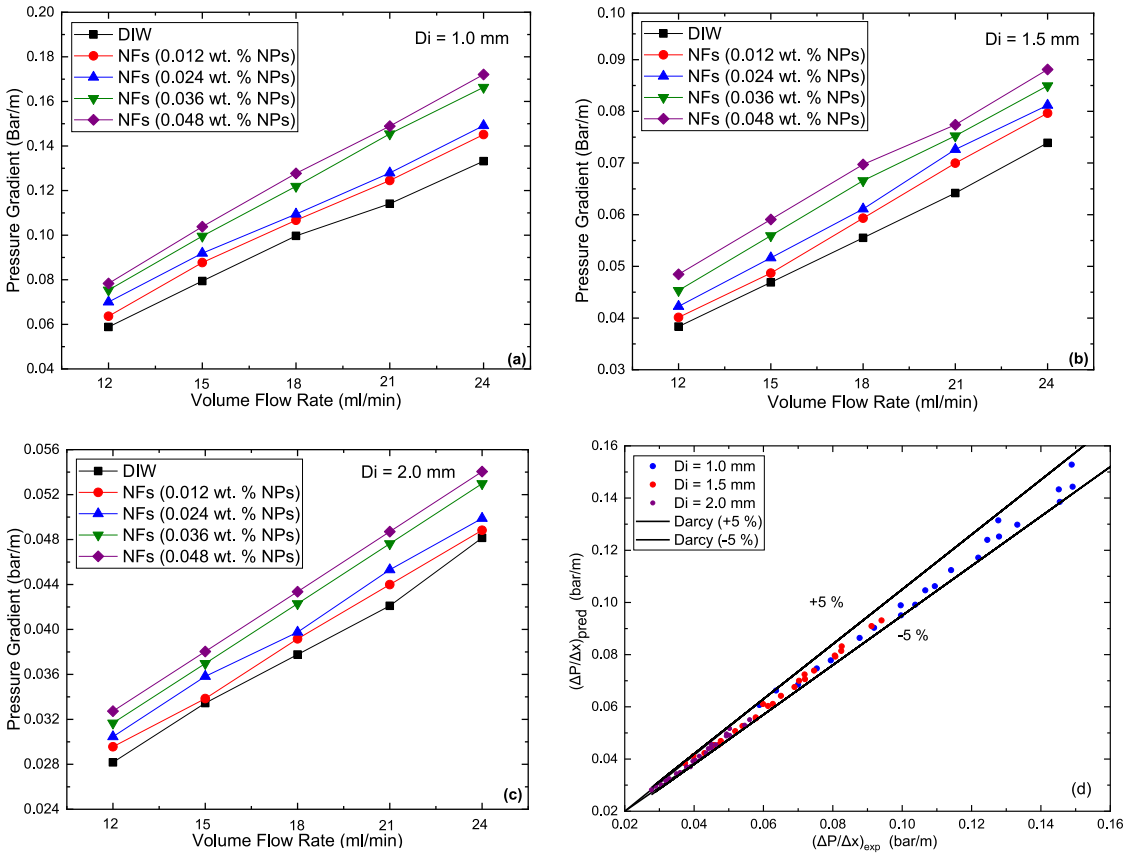

Fig. 11. Pressure gradient of ZnO-DIW as the function of volume flow rate (a) Di = 1.0 mm (b) Di = 1.5 mm (c) Di = 2.0 mm (d) Comparison with Darcy correlation prediction with experimental results.

Nevertheless, this decrement was not significant, and there is a potential for the future to optimize the test section diameters to create a balance between the tube cross-sectional area and enhancement in HTC. Optimized operating conditions could be determined for the enhanced thermal and hydraulic performance of the NFs in minichannel heat exchangers for high-tech modern thermal systems.

Author statement

Conceptualization: Habib-ur-Rehman Siddiqi and Adnan Qamar.
Methodology: Adnan Qamar, Rabia Shaukat, Zahid Anwar and Hassan Ali.
Formal analysis: Muhammad Mujtaba Abbas and Fahad Noor.
Investigation: Habib-ur-Rehman Siddiqi and Adnan Qamar.
Writing - Original Draft: Habib-ur-Rehman Siddiqi and Adnan Qamar.
Writing - Review & Editing: Muhammad Amjad, Muhammad Farooq, Hafiz Muhammad Ali, M.A. Kalam, T. M. Yunus Khan and Manzoore Elahi M. Soudagar.
Supervision: Shahid Imran.
Funding acquisition: T. M. Yunus Khan.

Declaration of competing interest

The authors declare that they have no known competing financial interests or personal relationships that could have appeared to influence the work reported in this paper.

Data availability

Data will be made available on request.

Acknowledgement

The authors extend their appreciation to the Deanship of Scientific Research at King Khalid University for funding this work through research groups program under Grant number (R.G.P. 2/105/43). In the current research work, the authors would like to thank the University of Engineering and Technology, Lahore, Pakistan, for funding the reported work under Research Grant No. ORIC/105-ASRB/3084, ORIC/101-ASRB/4452 and ORIC/101-ASRB/4453.

References

[1] M. Bahiraei, S. Heshmatian, Electronics cooling with nanofluids: a critical review, Energy Convers. Manag. 172 (July) (2018) 438–456, https://doi.org/10.1016/j.enconman.2018.07.047.
[2] A. Ijam, R. Saidur, Nanofluid as a coolant for electronic devices (cooling of electronic devices), Appl. Therm. Eng. 32 (2012) 76–82, https://doi.org/10.1016/j.applthermaleng.2011.08.032.
[3] R.B. Ganvir, P. V Walke, V.M. Kriplani, Heat transfer characteristics in nano fluid-A review, Renew. Sustain. Energy Rev. 75 (October 2016) (2017) 451–460, https://doi.org/10.1016/j.rser.2016.11.010.
[4] K.H. Solangi, et al., A comprehensive review of thermo-physical properties and convective heat transfer to nanofluids, Energy 89 (2015) 1065–1086, https://doi.org/10.1016/j.energy.2015.06.105.
[5] R. Saidur, K.Y. Leong, H.A. Mohammad, A review on applications and challenges of nanofluids, Renew. Sustain. Energy Rev. 15 (3) (2011) 1646–1668, https://doi.org/10.1016/j.rser.2010.11.035.
[6] A.J. Chamkha, M. Molana, A. Rahnama, F. Ghadami, On the nanofluids applications in microchannels: a comprehensive review, Powder Technol. 332 (2018) 287–322, https://doi.org/10.1016/j.powtec.2018.03.044.
[7] P. Nitiapiruk, O. Mahian, A.S. Dalkilic, S. Wongwises, Performance characteristics of a microchannel heat sink using TiO2/water nanofluid and different thermophysical models, Int. Commun. Heat Mass Tran. 47 (2013) 98–104, https://doi.org/10.1016/j.icheatmasstransfer.2013.07.001.
[8] E.B. Haghighi, et al., Cooling performance of nanofluids in a small diameter tube, Exp. Therm. Fluid Sci. 49 (2013) 114–122, https://doi.org/10.1016/j.expthermflusci.2013.04.009.
[9] H.A. Mohammed, G. Bhaskaran, N.H. Shuaib, R. Saidur, Heat transfer and fluid flow characteristics in microchannels heat exchanger using nanofluids: a review, Renew. Sustain. Energy Rev. 15 (3) (2011) 1502–1512, https://doi.org/10.1016/j.rser.2010.11.031.
[10] K.S. Hwang, S.P. Jang, S.U.S. Choi, Flow and convective heat transfer characteristics of water-based Al2O3 nanofluids in fully developed laminar flow regime, Int. J. Heat Mass Tran. 52 (1–2) (2009) 193–199, https://doi.org/10.1016/j.ijheatmasstransfer.2008.06.032.
[11] M. Karimzadehkhouei, S.E. Yalcin, K. Şendur, M. Pinar Mengüç, A. Koşar, Pressure drop and heat transfer characteristics of nanofluids in horizontal microtubes under thermally developing flow conditions, Exp. Therm. Fluid Sci. 67 (2015) 37–47, https://doi.org/10.1016/j.expthermflusci.2014.10.013.
[12] T. Wen, L. Lu, H. Zhong, B. Shen, Thermal properties measurement and performance evaluation of water/ZnO nanofluid in a mini channel with offset fins, Int. J. Heat Mass Tran. 162 (2020), 120361, https://doi.org/10.1016/j.ijheatmasstransfer.2020.120361.
[13] M.S. Lodhi, T. Sheorey, G. Dutta, Single-phase Fluid Flow and Heat Transfer Characteristics of Nanofluid in a Circular Microchannel : Development of Flow and Heat Transfer Correlations, 2020, pp. 1–20, https://doi.org/10.1177/0954406220916537, 0, no. 0.
[14] A. Azari, M. Kalbasi, M. Derakhshandeh, M. Rahimi, An experimental study on nanofluids convective heat transfer through a straight tube under constant heat flux, Chin. J. Chem. Eng. 21 (10) (2013) 1082–1088, https://doi.org/10.1016/S1004-9541(13)60618-7.
[15] H. Almohammadi, S.N. Vatan, E. Esmaeilzadeh, A. Motezaker, A. Nokhosteen, Experimental investigation of convective heat transfer and pressure drop of Al2O3/water nanofluid in laminar flow regime inside a circular tube, World Acad. Sci. Eng. Technol. 68 (8) (2012) 2208–2213.
[16] C.T. Nguyen, G. Roy, C. Gauthier, N. Galanis, Heat Transfer Enhancement Using Al2O3-Water Nanofluid for an Electronic Liquid Cooling System, vol. 27, 2007, pp. 1501–1506, https://doi.org/10.1016/j.applthermaleng.2006.09.028.
[17] M. Behi, et al., Experimental and numerical investigation on hydrothermal performance of nanofluids in micro-tubes, Energy 193 (2020), 116658, https://doi.org/10.1016/j.energy.2019.116658.
[18] S.M. Fotukian, M.N. Esfahany, Experimental study of turbulent convective heat transfer and pressure drop of dilute CuO/water nanofluid inside a circular tube, Int. Commun. Heat Mass Tran. 37 (2) (2010) 214–219, https://doi.org/10.1016/j.icheatmasstransfer.2009.10.003.
[19] M. Saeed, M. Kim, Heat transfer enhancement using nanofluids (Al2O3-H2O) in mini-channel heatsinks, Int. J. Heat Mass Tran. 120 (2018) 671–682, https://doi.org/10.1016/j.ijheatmasstransfer.2017.12.075.
[20] M.A.N. Hafiz Muhammad Ali, Hassan Ali, Liaquat Hassan, Hafiz Talha Bin Maqsood, Experimental investigation of convective heat transfer augmentation for car radiator using ZnO/water nanofluids, Energy 84 (2015) 317–324, https://doi.org/10.1016/j.energy.2015.02.103.
[21] W. Arshad, H.M. Ali, Experimental investigation of heat transfer and pressure drop in a straight minichannel heat sink using TiO2 nanofluid, Int. J. Heat Mass Tran. 110 (2017) 248–256, https://doi.org/10.1016/j.ijheatmasstransfer.2017.03.032.
[22] M.R. Sohel, S.S. Khaleduzzaman, R. Saidur, A. Hepbasli, M.F.M. Sabri, I.M. Mahbubul, An experimental investigation of heat transfer enhancement of a minichannel heat sink using Al2O3-H2O nanofluid, Int. J. Heat Mass Tran. 74 (2014) 164–172, https://doi.org/10.1016/j.ijheatmasstransfer.2014.03.010.
[23] A.H. Meghdadi Isfahani, M. Afrand, Experiment and Lattice Boltzmann numerical study on nanofluids flow in a micromodel as porous medium, Phys. E Low-Dimensional Syst. Nanostructures 94 (June) (2017) 15–21, https://doi.org/10.1016/j.physe.2017.07.008.
[24] A. Zarei, A. Karimipour, A.H. Meghdadi Isfahani, Z. Tian, Improve the performance of lattice Boltzmann method for a porous nanoscale transient flow by provide a new modified relaxation time equation, Phys. A Stat. Mech. its Appl. 535 (2019), 122453, https://doi.org/10.1016/j.physa.2019.122453.
[25] H. Azimy, A.H. Meghdadi Isfahani, M. Farahnakian, Investigation of the effect of ultrasonic waves on heat transfer and nanofluid stability of MWCNTs in sono heat exchanger: an experimental study, Heat Mass Transf. und Stoffuebertragung 58 (3) (2022) 467–479, https://doi.org/10.1007/s00231-021-03126-6.
[26] T. Wen, G. Zhu, K. Jiao, L. Lu, Experimental study on the thermal and flow characteristics of ZnO/water nanofluid in mini-channels integrated with GA-optimized ANN prediction and CFD simulation, Int. J. Heat Mass Tran. 178 (2021), 121617, https://doi.org/10.1016/j.ijheatmasstransfer.2021.121617.
[27] T. Wen, G. Zhu, L. Lu, Experimental and artificial neural network based study on the heat transfer and flow performance of ZnO-EG/water nanofluid in a mini-channel with serrated fins, Int. J. Therm. Sci. 170 (June) (2021), 107149, https://doi.org/10.1016/j.ijthermalsci.2021.107149.
[28] H.H. Balla, A.L. Hashem, Z.S. Kareem, A.F. Abdulwahid, Heat transfer potentials of ZnO/water nanofluid in free impingement jet, Case Stud. Therm. Eng. 27 (May) (2021), 101143, https://doi.org/10.1016/j.csite.2021.101143.
[29] T. Wen, L. Lu, S. Zhang, H. Zhong, Experimental study and CFD modelling on the thermal and flow behavior of EG/water ZnO nanofluid in multiport mini channels, Appl. Therm. Eng. 182 (August 2020) (2021), 116089, https://doi.org/10.1016/j.applthermaleng.2020.116089.
[30] W. Ahmed, et al., Characteristics investigation on heat transfer growth of sonochemically synthesized ZnO-DW based nanofluids inside square heat exchanger, J. Therm. Anal. Calorim. 144 (4) (2021) 1517–1534, https://doi.org/10.1007/s10973-020-09593-z.
[31] V.A. Martínez, F. Lozano-Steinmetz, D.A. Vasco, P.A. Zapata, I. Chi-Durán, D.P. Singh, Thermal characterization and stability analysis of aqueous ZnO-based nanofluids numerically implemented in microchannel heat sinks, Therm. Sci. Eng. Prog. 22 (2021), 100792, https://doi.org/10.1016/j.tsep.2020.100792.
[32] A. Qamar, Z. Anwar, H. Ali, S. Imran, R. Shaukat, M. Mujtaba Abbas, Experimental investigation of dispersion stability and thermophysical properties of ZnO/DIW nanofluids for heat transfer applications, Alex. Eng. J. 61 (5) (2022) 4011–4026, https://doi.org/10.1016/j.aej.2021.09.028.
[33] S.K. Sharma, S. Mital, Preparation and evaluation of stable nanofluids for heat transfer application: a review, Exp. Therm. Fluid Sci. 79 (2016) 202–212, https://doi.org/10.1016/j.expthermflusci.2016.06.029.
[34] A. Qamar, et al., Preparation and dispersion stability of aqueous metal oxide nanofluids for potential heat transfer applications: a review of experimental studies, J. Therm. Anal. Calorim. (2020), 0123456789, https://doi.org/10.1007/s10973-020-10372-z.

[35] X. Li, D. Zhu, X. Wang, Evaluation on dispersion behavior of the aqueous copper nano-suspensions, J. Colloid Interface Sci. 310 (2007) 456–463, https://doi.org/10.1016/j.jcis.2007.02.067.
[36] X. Wei, L. Wang, Synthesis and thermal conductivity of microfluidic copper nanofluids, Particuology 8 (3) (2010) 262–271, https://doi.org/10.1016/j.partic.2010.03.001.
[37] G. Paul, M. Chopkar, I. Manna, P.K. Das, Techniques for measuring the thermal conductivity of nanofluids: a review, Renew. Sustain. Energy Rev. 14 (2010) 1913–1924, https://doi.org/10.1016/j.rser.2010.03.017.
[38] M.L. Lemmon, E. McLinden, M.O. Huber, NIST reference fluid thermodynamic and transport properties-REFPROP, Chem. Prop 23 (2002) v7.
[39] E.C. Okonkwo, et al., *An Updated Review of Nanofluids in Various Heat Transfer Devices*, No. March, Springer International Publishing, 2020.
[40] U. Rea, T. Mckrell, L. Hu, J. Buongiorno, Laminar convective heat transfer and viscous pressure loss of alumina-water and zirconia-water nanofluids, Int. J. Heat Mass Tran. 52 (2009) 2042–2048, https://doi.org/10.1016/j.ijheatmasstransfer.2008.10.025.
[41] Y.I.C. Bock Choon Pak, Hydrodynamic and heat transfer study of dispersed fluids with submicron metallic oxide, *Exp. Heat Transf. A J. , Therm. Energy Transp. , Storage , Convers.*, no. January 2013 (2013) 37–41.
[42] M.M. Heyhat, F. Kowsary, A.M. Rashidi, S. Alem Varzane Esfehani, A. Amrollahi, Experimental investigation of turbulent flow and convective heat transfer characteristics of alumina water nanofluids in fully developed flow regime, Int. Commun. Heat Mass Tran. 39 (8) (2012) 1272–1278, https://doi.org/10.1016/j.icheatmasstransfer.2012.06.024.
[43] W. Ahmed, Z.Z. Chowdhury, S.N. Kazi, M.R. Johan, N. Akram, C.S. Oon, Effect of ZnO-water based nanofluids from sonochemical synthesis method on heat transfer in a circular flow passage, Int. Commun. Heat Mass Tran. 114 (2020), 104591, https://doi.org/10.1016/j.icheatmasstransfer.2020.104591.
[44] B. Sahin, E. Manay, E.F. Akyurek, An experimental study on heat transfer and pressure drop of CuO-water nanofluid, J. Nanomater. 2015 (October) (2015), https://doi.org/10.1155/2015/790839.
[45] N. Kumar, S.S. Sonawane, Convective Heat Transfer of Metal Oxide-Based Nanofluids in a Shell and Tube Heat Exchanger, 2018, pp. 183–192, https://doi.org/10.1007/978-981-10-6107-3_14.
[46] R.B. Ananthu C Mohan, Preparation of zinc oxide nanoparticles and its characterization using scanning Electron microscopy (SEM) and X-ray diffraction(XRD), Procedia Technol 24 (2016) 761–766.
[47] J. Bayat, A.H. Nikseresht, Thermal performance and pressure drop analysis of nanofluids in turbulent forced convective flows, Int. J. Therm. Sci. 60 (2012) 236–243, https://doi.org/10.1016/j.ijthermalsci.2012.04.012.
[48] G.J. Lee, C.K. Kim, M.K. Lee, C.K. Rhee, S. Kim, C. Kim, Thermal conductivity enhancement of ZnO nanofluid using a one-step physical method, Thermochim. Acta 542 (2012) 24–27, https://doi.org/10.1016/j.tca.2012.01.010.
[49] K.E. Ramohlola, E.I. Iwuoha, M.J. Hato, K.D. Modibane, Instrumental techniques for characterization of molybdenum disulphide nanostructures, J. Anal. Methods Chem. 2020 (1) (2020), https://doi.org/10.1155/2020/8896698.
[50] M. Naderi, Surface area: brunauer-emmett-teller (BET), Prog. Filtr. Sep. (2015) 585–608, https://doi.org/10.1016/B978-0-12-384746-1.00014-8.
[51] T.T. Loong, H. Salleh, A. Khalid, H. Koten, Thermal performance evaluation for different type of metal oxide water based nanofluids, Case Stud. Therm. Eng. 27 (July) (2021), 101288, https://doi.org/10.1016/j.csite.2021.101288.
[52] R.V. Pinto, F.A.S. Fiorelli, Review of the mechanisms responsible for heat transfer enhancement using nanofluids, Appl. Therm. Eng. 108 (2016) 720–739, https://doi.org/10.1016/j.applthermaleng.2016.07.147.
[53] J.C. Maxwell, A treatise on electricity and magnetism, in: third ed.A Treatise Electr. Magn., vol. 53, Clarendon Press, Oxford, UK, 1891, pp. 1–30, https://doi.org/10.1017/CBO9781107415324.004, 1954.
[54] R.L. Hamilton, O.K. Crosser, Thermal conductivity of heterogeneous two-component systems, Ind. Eng. Chem. Fundam. 1 (3) (1962) 187–191, https://doi.org/10.1021/i160003a005.
[55] E.V. Timofeeva, et al., Thermal conductivity and particle agglomeration in alumina nanofluids: experiment and theory, Phys. Rev. E - Stat. Nonlinear Soft Matter Phys. 76 (6) (2007) 28–39, https://doi.org/10.1103/PhysRevE.76.061203.
[56] E.J. Wasp, J.P. Kenny, R.L. Gandhi, Solid-liquid flow: slurry pipeline transportation, [Pumps, valves, mechanical equipment, economics] 1 (1977). United States).
[57] H.A. Mintsa, G. Roy, C.T. Nguyen, D. Doucet, New temperature dependent thermal conductivity data for water-based nanofluids, Int. J. Therm. Sci. 48 (2) (2009) 363–371, https://doi.org/10.1016/j.ijthermalsci.2008.03.009.
[58] A. Einstein, A new determination of molecular dimensions, Ann. Phys. 19 (1906) 289–306.
[59] X. Xu, S.U.S. Choi, X. Wang, Thermal conductivity of nanoparticle - fluid mixture, J. Thermophys. Heat Tran. 13 (4) (1999) 474–480.
[60] O.A. Alawi, N. Azwadi, C. Sidik, H. Wei, T. Hao, S.N. Kazi, Thermal conductivity and viscosity models of metallic oxides nanofluids, Int. J. Heat Mass Tran. 116 (2018) 1314–1325.
[61] L.A. Dávalos Orozco, L.F. del Castillo, Hydrodynamic Behavior of Suspensions of Polar Particles, third ed., Encycl. Surf. Colloid Sci., 2016, pp. 3070–3091, https://doi.org/10.1081/e-escs3-120021916.
[62] K.P. Venkitaraj, S. Suresh, T. Alwin Mathew, B.S. Bibin, J. Abraham, An experimental investigation on heat transfer enhancement in the laminar flow of water/TiO2 nanofluid through a tube heat exchanger fitted with modified butterfly inserts, Heat Mass Transf. und Stoffuebertragung 54 (3) (2018) 813–829, https://doi.org/10.1007/s00231-017-2174-5.
[63] M. Qasim, M. Sajid Kamran, M. Ammar, M. Ali Jamal, M. Yasar Javaid, Heat transfer enhancement of an automobile engine radiator using ZnO water base nanofluids, J. Therm. Sci. 29 (4) (2020) 1010–1024, https://doi.org/10.1007/s11630-020-1263-9.
[64] E.B. Haghighi, et al., Cooling performance of nanofluids in a small diameter tube, Exp. Therm. Fluid Sci. 49 (2013) 114–122, https://doi.org/10.1016/j.expthermflusci.2013.04.009.